CHAPTER-3

Details of Experimental Techniques

In this chapter we discuss the materials used, preparation method of the samples, various characterization techniques employed to study the prepared samples and irradiation.

INTRODUCTION

In this chapter we will discuss the method of synthesizing the polymer blend electrolyte samples and explain certain theories of the characterization techniques. Complex Impedance Analysis was used to study the dielectric properties of the electrolytes and the other experimental techniques undertaken in the present study include *Fourier transform infrared spectroscopy (FT-IR), X-ray diffraction (XRD), Differential Scanning Calorimetry (DSC), Scanning electron microscope (SEM) and Transference Number Measurement.*

3.1 Materials and methods

3.1.1 The technical details of the materials used for the present studies are given below in the table (Table 3.1).

Table 3.1 Technical details of the materials used.

Sr. No	Name of the Material	Structure	Type	Glass transition temperature T_g (^{0}C)	Make
1	Poly (ethylene oxide) (PEO) Mol. wt. 3 x 10^5 $gmol^{-1}$	$-(CH_2 - CH_2 - O-)_n$	Polymer	-60	Alfa Aesar (U.S.A)
2	Polyacrylamide (PAM) Mol. wt. 5 x 10^6 $gmol^{-1}$	$-(-CH_2CHCONH_2-)_n$	Polymer	438	HiMedia
3	Sodium triflormethanesufonate (Sodium triflate) Mol. wt. 172.06 $gmol^{-1}$	$NaCF_3SO_3$	Salt	253-255	Sigma Aldrich
4	Ethylene Carbonate Mol. wt. 88.06 $gmol^{-1}$	$C_3H_4O_3$	Plasticizer	35- 38	Aldrich
5	Propylene Carbonate Mol. wt. 102.09 $gmol^{-1}$	$C_4H_6O_3$	Plasticizer	55	Sigma Aldrich
6	Silicon dioxide particles	SiO_2	Nano filler		Sigma Aldrich
7	Deionised Water	H_2O	Common Solvent	-	-

Poly (ethyleneoxide) (PEO

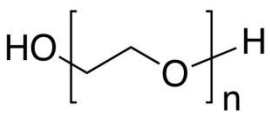

Fig. 3.1 *Structure of Poly (ethylene oxide) (PEO).*

Polyethyleneoxide (PEO) is a white powder with no typical smell and about 70-85% crystallinity. It is an in amorphous elastomer phase at room temperature ***(Belfiore, 2010; Raff and Ahmad, 1970; Dorest, 1994; Sharma, 2013)***. It is partially crystalline in nature which is a major drawback for its applications in polymer electrolytes. PEO has a spherulitic crystalline structure with defined amorphous boundary ***(Raff and Ahmad, 1970)***. Overall morphology of PEO presents it as an important candidate as a host matrix for electrolyte materials ***(Kim and Kim, 1999)***. PEO has a linear structure and the ether oxygen atoms have enough electro-negativity to bond strongly with large cationic groups of ionic salts. PEO has been known to dissolve most alkali metal ion salts easily. Highly flexible chain dynamics of PEO make it an outstanding choice for electrolyte host.

Polyacrylamide (PAM)

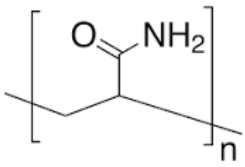

Fig. 3.2 *Structure of Polyacrylamide (PAM).*

PAM (polyacrylamide) is a highly amorphous polymer and generally used for production of lenses and in waste management systems. Only a few reports exist on its use as an electrolyte. Negligible corrosive nature, high compatibility with many electrodes and current collectors and wide potential window are some of the important advantages of neutral pH PAM ***(Virya and Lian, 2017)***. PAM possesses quintessential 3D-network structure and a high degree of cross-linking. Apart from this PAM also has excellent colloidal stability ***(Tang et al., 2008)***. This makes it a very interesting constituent in electrolyte applications. When dissolved in water, PAM becomes soft hydrogel which makes the entire system quiet flexible and a better ion transport can be expected.

Sodium triflоromethanesufonate (Sodium triflate)

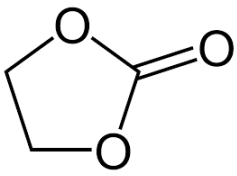

Fig. 3.3 *Structure of Sodium triflate ($NaCF_3SO_3$).*

Triflate anion, $CF_3SO_3^-$, is an extremely stable polyatomic ion and is the conjugate base of Triflic acid, CF_3SO_3H. Triflate group is an excellent leaving group and hence can quickly get attached to the polymer chains. Sodium has very well established itself as a competent candidate as compared to other metal ion electrolytes due to its material abundance, low cost and environment friendly nature.

Ethylene Carbonate (EC)

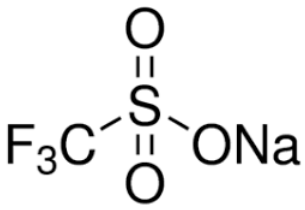

Fig. 3.4 *Structure of Ethylene Carbonate (EC).*

Ethylene Carbonate (EC) is the carbonate ester of ethylene glycol and carbonic acid. At room temperature (25 °C) ethylene carbonate is a transparent crystalline solid, essentially odourless and colourless and up to some extent water soluble. Ethylene carbonate is commonly used as a polar solvent and as high permittivity component of electrolytes in batteries. It has a high dielectric constant (89.78) and high boiling point (521 K) ***(Arunkumar et al., 2017)***, which plays a key role in its applications in electrolyte systems.

Propylene Carbonate (PC)

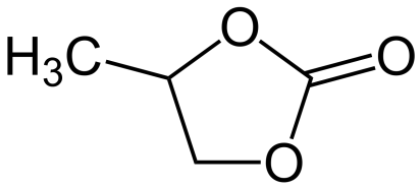

Fig. 3.5 *Structure of Propylene Carbonate (PC).*

It is a cyclic carbonate ester derived from propylene glycol and readily soluble in water. This colourless and odourless liquid is useful as a polar, aprotic solvent. Also due to its high dielectric constant (64), it is frequently used as a high-permittivity component of electrolytes for batteries.

Silicon dioxide particles (SiO_2)

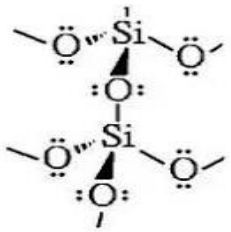

Fig. 3.6 *Structure of Silicon dioxide (SiO_2).*

Silicon dioxide nano particles appear in the form of a white powder and are important for research purposes due to their stability, low toxicity and ability to be functionalized with a range of molecules and polymers. Majorly used for applications in manufacturing of rubber and plastic, SiO_2 has also been widely used by researchers as a filler component in electrolytes for battery applications.

Deionized Water

Deionized water is free of ions, and it has no charge. It can be processed in laboratory by treating conventional water with electrically charged resins that will bind and attract to salts and remove them from the water. Deionized water is a true water blank, which means it assumes the chemistry of whatever product is added to it and this makes it a very good solvent for numerous industrial applications.

3.1.2 Sample Preparation Method

As mentioned before, all the samples were prepared using conventional solution cast technique In solution casting, the polymer is dissolved in a solvent and spread on an even surface where is allowed to dry. After all the solvent gets evaporated, stand-alone polymer film can be peeled off the casting surface.

Appropriate amounts of the polymers PEO and PAM were separately dissolved in de-ionized water, stirred for 24 h and then the mixture as a whole was taken with salt and stirred for further 24 h. Plasticizer ethylene carbonate (EC) was first brought to liquid state and then relevant amounts of EC and propylene carbonate (PC) plasticizers were added to the homogeneous solution and stirred for 24 h. For dispersion of nano-fillers, SiO_2 particles were first dispersed in de-ionized water and then the nano-dispersed liquid was added to the homogeneous gel and stirred for 24 h. After the final stirring,

homogeneous gel was casted onto teflon petri dish and allowed to dry at room temperature.

3.2 Blend Polymer Electrolyte (BPE) systems

In the present study, we have prepared polymer blend samples of PEO (polyethylene oxide) and PAM (polyacrylamide). Total mass of the blend is kept at 750 mg. The chemicals PEO, PAM, $NaCF_3SO_3$, EC, PC and nano-SiO_2 were used as received for synthesizing the polymer blend electrolytes. De-ionized water was used as common solvent and inorganic sodium triflate ($NaCF_3SO_3$) was used as metal ion salt for blend polymer films. The polymer blend electrolytes were prepared by conventional solution cast technique. The blend system of PEO and PAM was first synthesized without addition of any other component to deem the most appropriate ratio of the two polymers

1.2.1 First Blend Polymer Electrolytes System (PPS system)

First blend polymer electrolyte system was synthesized to analyze the effect of variation in salt concentration on the blend polymer system. The blend electrolytes were prepared as: 1: 1 (*w/w*) (PEO – PAM) + *x* wt% $NaCF_3SO_3$, *x* = 5 wt% - 17.5 wt% in steps of 2.5. These compositions and their legends are tabulated in table below (Table 3.2).

Table 3.2 Composition and legends for first series.

Sr.No.	Legends	PEO (wt %)	PAM (wt %)	$NaCF_3SO_3$ (wt%)
1	PPS-5	50	50	5
2	PPS-7.5	50	50	7.5
3	PPS-10	50	50	10
4	PPS-12.5	50	50	12.5
5	PPS-15	50	50	15
6	PPS-17.5	50	50	17.5

3.2.2 Second Blend Polymer Electrolyte System (PPSP system)

After deeming PPS-17.5 sample as optimum, in the second series was synthesized to observe the effect of various concentrations of plasticizer (EC+PC) in the blend polymer electrolyte system. The plasticized blend polymer electrolytes were prepared as:1: 1 (*w/w*) (PEO – PAM) – 12.5 wt% $NaCF_3SO_3$ + *x* wt% 1: 1 (*w/w*) (EC-PC), *x* = 5 wt% - 25 wt% in steps of 5.

These compositions and their legends are tabulated in table below (Table 3.3).

Table 3.3 Composition and legends for second series.

Sr. No.	Legends	PEO (wt %)	PAM (wt %)	$NaCF_3SO_3$ (wt%)	EC+PC (wt%)
1	PPSP-5	50	50	17.5	5
2	PPSP-10	50	50	17.5	10
3	PPSP-15	50	50	17.5	15
4	PPSP-20	50	50	17.5	20
5	PPSP-25	50	50	17.5	25

1.2.3 Third Blend Polymer Electrolyte System (PPSPN system)

PPSP-15 sample was optimized as highest conducting sample from the second series and then after, third series with varying concentration of nano-SiO_2 was synthesized to analyze its effect on the plasticized blend polymer electrolyte system. The nano-dispersed plasticized blend polymer electrolytes were prepared as: 1: 1 (*w/w*) (PEO – PAM) – 12.5 wt% $NaCF_3SO_3$ – 20 wt% (EC – PC) + *x* wt% SiO_2, *x* = 5 wt% -15 wt% in steps of 2.5

These compositions and their legends are tabulated in table below (Table 3.4).

Table 3.4 Composition and legends for third series.

Sr. No.	Legends	PEO (wt %)	PAM (wt %)	$NaCF_3SO_3$ (wt%)	EC+PC (wt%)	Nano-SiO_2 (wt%)
1	PPSPN-5	50	50	17.5	15	5
2	PPSPN-7.5	50	50	17.5	15	7.5
3	PPSPN-10	50	50	17.5	15	10
4	PPSPN-12.5	50	50	17.5	15	12.5
5	PPSPN-15	50	50	17.5	15	15

3.3 Irradiation

The irradiation of polymer electrolyte samples was carried out at the inter-university accelerator center (IUAC) New Delhi. The accelerator center provides beam line for applicatons in nuclear physics, atomic physics, materials science, biosciences and other allied fields. Inter-University Accelerator Centre has a running Pelletron, a tandem Van de graaf type accelerator. For present study we utilised the material science beam line of the Pelletron. A schematic diagram of the Pelletron is shown in Fig. 3.6 below.

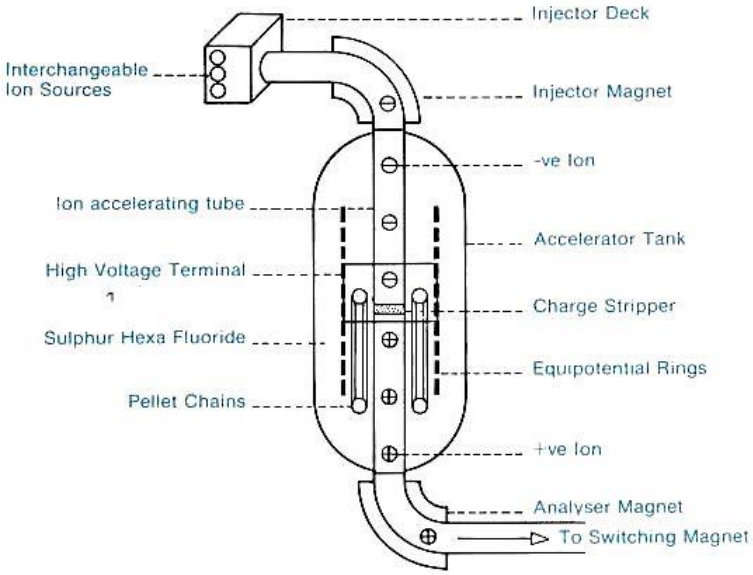

Fig. 3.7 *Schematic of Pelletron Acceleator, IUAC.*

In this machine, the negative ions are produced and pre-accelerated to ~300KeV in ion Source and injected into strong electrical field inside an accelerator tank filled with SF_6 insulating gas. At the centre of the tank is a terminal shell which is maintained at a high voltage (~15 MV). The negative ions on traversing through the accelerating tubes from the column top of the tank to the positive terminal get accelerated. On reaching the terminal they pass through a stripper which removes some electrons from the negative ions, thus transforming the negative ions into positive ions. These positive ions are then repelled away from the positively charged terminal and are accelerated to ground potential to the bottom of the tank. In this manner same terminal potential is used twice to accelerate the ions. On exiting from the tank, the ions are bent into horizontal plane by analyzing magnet, which also select a particular beam of ion. The switching magnet diverts the high energy ion beams into various beam lines into the different experimental areas of the beam hall. The entire machine is computer controlled and is operated from the control room (http://www.iuac.res.in/accel/pell/Accelerator.htm).

For ion beam irradiation, free standing films were cut into 1 cm × 1cm segments and mounted on the ladder maintaining distance of 1 cm between all the samples. Irradiation with 80 MeV swift heavy O^{6+} ion beam was carried out using material science beam line facility of pelletron accelerator at IUAC, New Delhi, India. Irradiation had taken place at room temperature for four different fluences of 1×10^{11}, 3×10^{11}, 1×10^{12} and

2×10^{12} ions/cm^2 and a constant current of 0.4 pnA (particle nano ampere) (flux) was maintained throughout the experiment.

3.4 Theoretical details of various characterization techniques

Different experimental techniques used to characterize the prepared polymer films are discussed briefly in the following sub-sections below.

3.4.1 Fourier Transform Infrared Spectroscopy (FT-IR)

Vibrational spectroscopy is extensively used for studying the modifications occurring in materials induced by ion beam irradiation and understanding the change in molecular bond lengths of the polymers or interaction between the constituents, if any. The IR spectra of the materials provide information about the occurrence of complexation also between various constituents ***(Ramesh et al., 2007)***. Absorption in the infrared region results in changes in vibrational and rotational status of the molecules. The absorption frequency depends on vibrational frequency of the molecule, and the absorption intensity leans onto, how sufficiently the infrared photon energy is transferred to the molecule which in turn depends on the change in the dipole moment which occurs as a consequence of molecular vibration. Wherefore, a molecule will absorb infrared light only when the absorption can lead to a change in its dipole moment. In a FTIR instrument, a Michelson type interferometer is used. A beam-splitter within the interferometer splits the beam of radiation into two. The two beams re-coalesce after a path difference is introduced between them. In this way, interference is achieved between the beams and the intensity of the output beam from the interferometer is obtained using an appropriate detector ***(Amand and Tullin, 1996)*** Fig. 3.7 shows schematic diagram of a typical FT-IR instrument.

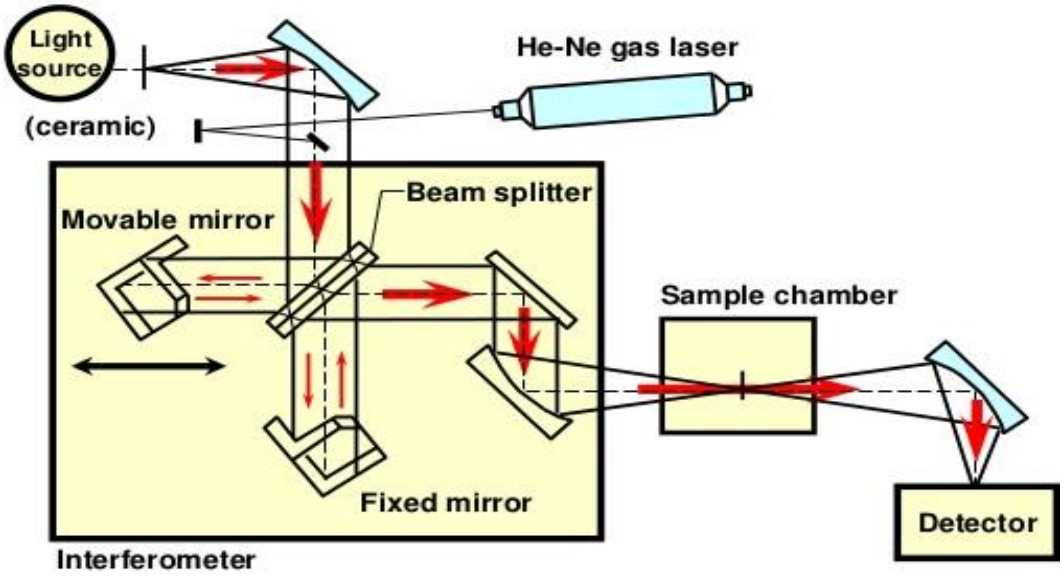

Fig. 3.8 *Schematic diagram of a typical FT-IR Instrument.*

The detector detects cosine wave, when the moving mirror gradually moves along the beam direction and the source emits single frequency. The resulting interferogram is made up of a strong signal at zero path difference point, which progressively falls off on either side. When the interferogram is treated by mathematical process of Fourier Transformation, single beam spectrum is produced. Normal functioning of interferometers is recording the background first and then rationing it against the sample spectrum which is inserted in the beam between the interferometer and detector. In the path of IR radiation through the sample, some of the infrared radiation gets absorbed by the sample and some of it is passes through (transmitted). The resulting molecular fingerprint of the sample represents the molecular spectrum of absorption and transmission. Like a fingerprint, two different molecular structures do not produce the same infrared spectrum. This makes infrared spectroscopy very important in diverse investigations.

A natural vibrational mode within a molecule absorbs IR radiation under the following conditions:

1) The natural frequency of vibration of the molecule is the same as the frequency of the incident radiation. The absorbed IR radiation causes the molecule to vibrate with larger amplitude (Resonance).

2) Molecules in which absorption produces some changes in its electric dipole, only those so called *"IR- active"* materials absorb IR radiation.

Molecule with an electric dipole, when exposed to electric field, is acted upon by the force of field which changes the separation of its charges. Periodic change in polarity of IR radiation is the consequence of change in its electric field. This signifies that the separation of the charged atoms of the molecule changes periodically vibrations of which, lead to the absorption of IR radiation by the molecule. Centres of gravity of the charges coincide in every vibrational position in a symmetrical stretching vibration so no dipole moment exists hence and the absorption characteristic of this mode is not observed in IR. These are "*IR-inactive"* vibrations. On the other hand, asymmetrical stretching vibration produces a net dipole moment and the IR-active vibration is observed in the spectrum.

Position of atoms in a molecule does remain fixed, they undergo diverse stretching and bending vibrations. Energy of vibration depends on atomic arrangement of the molecule, mass of the atoms and the bond strength. Position of IR band is expressed in terms of wavelength (λ, generally taken in *microns* unit) or the wave number, $\bar{\nu}$. Relation between these two can be given as

$$\bar{\nu}(cm^{-1}) = \frac{10^4}{\lambda}\ (in\ \mu) \qquad \textbf{(3.1)}$$

Position of the absorption bands can be derived from mechanical theory of harmonic oscillators as under:

$$\bar{\nu}(cm^{-1}) = \frac{1}{2\pi c}\sqrt{\frac{k\,(m_1+m_2)}{m_1 m_2}} \qquad \textbf{(3.2)}$$

where, m_1 and m_2 are the masses of two adjacent atoms in a molecule and *k*: the restoring force per unit displacement is expressed as

$$k = aN\left(\frac{\chi_1\chi_2}{d^2}\right)^{3/4} + b \qquad \textbf{(3.3)}$$

where, *N* stands for the band order (i.e., effective number of covalent or ionic bands), χ_1 and χ_2 are the electro negativities of the atoms, d is the inter-nuclear distance in angstroms and $a = 1.67, b = 0.3$ are constants.

Above relations clarify the role of bond length as guide to understand the direction of the shift of the band which results from changes in chemical group. Greater length suggests lower frequency.

Bending Vibrations:

The fundamental stretching modes produce higher frequency absorption bands as compared to bending vibrations. The two types of stretching modes viz., symmetric and asymmetric, arise as a consequence of stretching and contracting of bond without changing the bond angles. Movement of atoms, with respect to a particular atom in a molecule occurring in the same direction produces symmetrical stretching vibrations. In case of a tri-atomic molecule, one of the atoms approaches the central atom and the other moves away from it. The outer atom moves unequally with respect to the central atom. This leads to a change in electric dipole and hence asymmetric stretching vibration gives higher wave number than that given by the symmetric system.

In bending mode, the bond angles get deformed but there is no change in the corresponding lengths. For diatomic molecules, most of the bond angles are either in the proximity of linear-180^0 or in the proximity of 120^0-110^0. In case of tri-atomic molecules, two same atoms are bound to the central by equal bonds having different symmetric or asymmetric frequencies.

Theoretically, bending vibrations of a tri-atomic molecule can be derived as below:

$$\bar{v}_{sym}(cm^{-1}) \approx \left(\frac{1}{2\pi c}\right)\left[k\left\{\frac{1}{M_{end}} + \frac{(1+cos\,\alpha)}{M_{cen}}\right\}\right]^{1/2} \qquad \textbf{(3.4)}$$

$$\bar{v}_{asym}(cm^{-1}) \approx \left(\frac{1}{2\pi c}\right)\left[k\left\{\frac{1}{M_{end}} + \frac{(1-cos\,\alpha)}{M_{cen}}\right\}\right]^{1/2} \qquad \textbf{(3.5)}$$

where, α is the bond angle, v is the frequency in cm^{-1}, k is the force constant taken in dyne/cm, M_{end} and M_{cen} are the atomic weights of end atom and central atoms respectively.

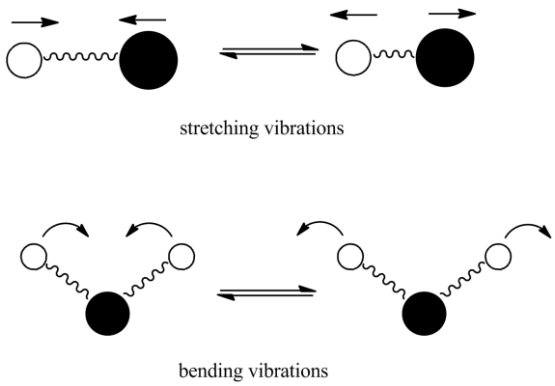

Fig. 3.9 *Stretching vibrations of a diatomic molecule and bending vibrations of a triatomic molecule.*

Bending vibrations are classified into four types.

1. **Scissoring**: In scissoring mode of bending vibrations, the two atoms approach each other in the same plane.
2. **Twisting**: Twisting vibrations result due to motion of one of the atoms above the plane and the motion of the other atom below the plane of the central atom.
3. **Wagging:** In this mode, the vibration occurs due to up and down motion of the two atoms below the plane of the central atom.
4. **Rocking:** In rocking mode, the motion of the atoms occur in the same direction and in the same plane.

All the above discussed bending vibrations are shown in the figure below. In the figures, (+ve) and (–ve) signs are respectively used to represent the motion of the atoms above and below the plane of the paper.

Fourier transformation of the obtained IR spectrum is a very important feature from application point of view. When collected over FT-IR, the infrared spectra are highly precise as well as accurate. The internal precision and accuracy of the wavelength positions are set by laser which are monitors the motion of the moving mirror and data collection time. Unlike a dispersive spectrometer, FT-IR spectrometer does not separate the energy into individual frequencies, each point in the interferogram encompasses information from each wavelength of light being measured and thus a multiplex spectrum results. Less reflection losses in IR spectra are found when scanned on FT-IR spectrometer as compared to the dispersive spectrometer. This account for higher signal-to-noise ratio, better sensitivity of smaller peaks, higher resolution and more perceptible features.

The image of the FT-IR instrument used in the present study is shown below (Fig. 3.9(b)).

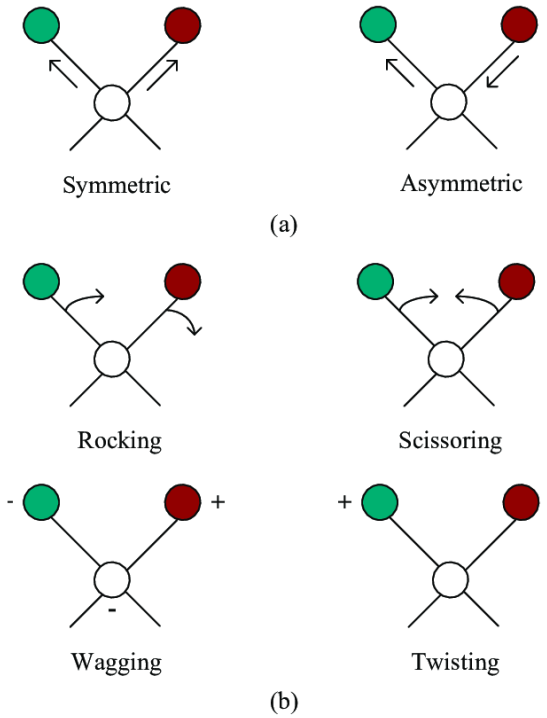

Fig. 3.10(a) *Different types of Bending vibrations of a triatomic molecule.*

Fig. 3.10(b) *Image of FT-IR instrument.*

(FT-IR 4100 JASCO model)

3.4.2 X-Ray Diffraction Analysis (XRD)

Structural properties of a material depicting its crystalline nature, amorphous volume and crystallite size are studied using the XRD analysis. For diffraction purposes, short wavelength X-rays in the range of few angstroms are used. The wavelength of X-rays is comparable to the atomic size and hence the best suited to probe structural organization of diversified materials. Electron beam accelerated with high voltage when bombards on a stationary or moving target, produces X-rays. Commonly used targets

for generation of X-rays include Copper (Cu) which gives 8 keV X-rays of 1.54 $\dot{A}$ wavelength and Molybdenum (Mo) giving 14 keV X-rays with 0.8 $\dot{A}$ wavelength. Diffraction takes place when atomic planes of a crystal cause interference of incident X-ray beams with each other as they are leaving the crystal plane. Diffraction peaks are directly related with atomic distance. For a particular set of lattice plane with inter-planar spacing *d*, diffraction condition is defined as Bragg's Law (condition) given as in equation 3.6 below.

$$n\lambda = 2d\ sin\theta \qquad \textbf{(3.6)}$$

where, n is a number representing order of diffraction peaks, λ is the wavelength of the incoming X-ray in $\dot{A}$, d is the inter-atomic spacing in $\dot{A}$ and θ is the diffraction angle taken in degrees.

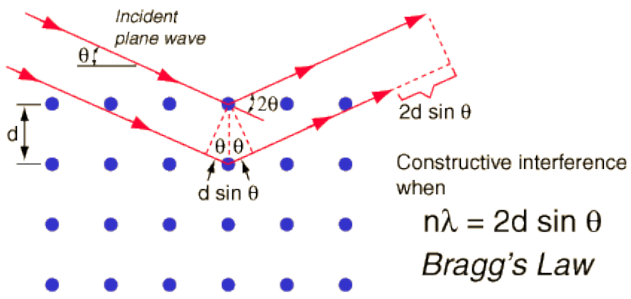

Fig. 3.11 *Bragg's Law.*

For crystals, the diffractogram is in the form of sharp and intense peaks which have same symmetry as that of the atom whereas diffraction patterns are in the form of few diffused halos instead for amorphous samples. Thus the resulting diffraction pattern, enable us to understand the atomic distribution in materials. XRD is based on the constructive interference of monochromatic x-rays from a crystalline sample. These x-rays are generated by a cathode ray tube which is filtered to produce monochromatic radiation, collimated to focus and aimed at the sample under investigation. Diffracted ray is produced as a consequence of constructive interference of the incident rays with the sample when conditions satisfy Bragg's condition as per equation 3. 6. These diffracted x-rays are then detected, processed and counted by scanning the sample through a range of 2θ angles.

The image of the FT-IR instrument used in the present study is shown below (Fig. 3.11).

(Bruker X-ray diffractometer, Model D8)

Fig. 3.12 *Image of X-ray Diffraction instrument.*

3.4.3 Scanning Electron Microscopy (SEM)

The Scanning Electron Microscopy (SEM) analysis is widely used to understand the properties of solid materials such as morphology, structure and crystallite size which are used to probe the defect chemistry at the surface and understand the dissemination of constituents in the material. Fig. 3.12 shows schematic of the scanning microscope.

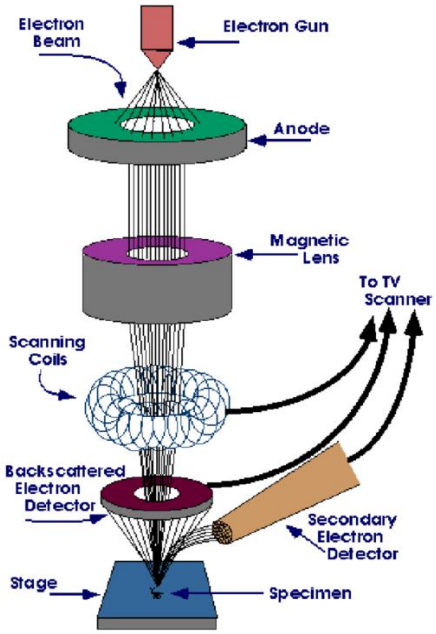

Fig. 3.13 *Working Principle of SEM instrument.*

Main components of a typical SEM are electron gun, condenser lens, scan coil, detectors, specimen and lenses. An electron beam is generated by heating the tungsten

filament and then directed at the specimen. Presence of high vaccum confirms negligible interaction between the electron beam and the atmospheric particles. The finely tuned beam of electrons scans the surface of the specimen over a very small area. Incident electron beam is scattered in the sample elastically or in-elastically (back-scattering). This gives rise to various signals which can be detected by the detector which give out the topographic information about the specimen. SEM image thus obtained will present the distribution of different chemical phases present on the specimen surface. Resolution of the image is not of good quality as that obtained in the case of secondary electrons, hence low-energy secondary electron emission technique is more generally accepted mode of operation of SEM. Low-energy electrons are generated when primary electrons enter the specimen surface with an energy of 0.5-30 keV. The sample image is built up as a variation in secondary electron intensity with respect to position of the scanning primary electron beam which can be focussed to a very small spot to obtain high spatial resolution.

Fig. 3.14 *Image of the gold/palladium source coating unit for SEM studies.*

(JOEL JSM-6380LV, SEM Instrument)

Fig. 3.15 *Image of SEM Microscope.*

3.4.4 Differential Scanning Calorimetry (DSC)

Thermal analysis techniques like Differential Scanning Calorimetry (DSC), Differential Thermal Analysis (DTA), Thermo-gravimetric Analysis (TGA) and Dynamic Mechanical Analysis (DMA) are some of the commonly used techniques to probe the thermal behaviour of the materials. In each of these methods, the sample under investigation is exposed in a controlled temperature environment programmed to increase or decrease or stay constant.

DSC is a thermo-analytical technique widely used to investigate physical and thermal properties of polymer materials. The difference in the amount of heat required to

increase the temperature of the sample with respect to a reference is measured as a function of increasing temperature. DSC measures the amount of heat released by a sample when the temperature is increased or decreased in a controlled manner. The reference sample should be so chosen which has well defined heat capacity over the range of temperatures to be scanned and generally the reference used is an empty pan or a pan containing some inert material such as anhydrous alumina. The sample and reference have individual heaters and both the reference and the sample are maintained at nearly equal temperature throughout the experiment. The temperature program in DSC is devised such that the temperature of the sample holder increases linearly with time. When the sample undergoes physical changes such as phase transformation or melting of the sample, less (or more) heat is required to flow through the sample as compared to the reference. And this is decided on the basis whether the process is endothermic or exothermic in nature. If a solid sample undergoes melting by absorption of heat (endothermic process) then more heat is required to flow to the sample at the same rate as that of reference. In case of exothermic process like crystallization phenomenon, less heat should flow to the sample. During such transitions, amount of heat released or absorbed is measured by differential scanning calorimeters by observing the difference in heat flow between the sample and the reference. As shown in the figure, in a typical DSC experiment, the DSC cell which is a metallic disc made of an alloy of constantan serves as primary source of heat transfer from and to the sample and the reference. Sample contained in a metal pan and the reference pan are both placed on an elevated platform formed on thermodynamic disc. When the heat is transferred to the disc, the differential heat flowing through the sample and the reference is measured by the thermocouples formed from the junction of disc and chromel wafers which cover the underside of the platforms. These thermocouples are connected in series and measure the differential heat flow using the thermal equivalent of ohms written as: $\frac{dQ}{dt} = \frac{\Delta T}{R_D}$ ***(3.7)***

where, $\frac{dQ}{dt}$ is the heat flow, ΔT is the difference in temperatures of sample and reference and R_D is the thermal resistance of the disc.

DSC experiment results in a heat curve versus temperature as shown in Fig. 3.16. The endothermic peak symbolizes absorption of heat and exothermic peak shows heat released.

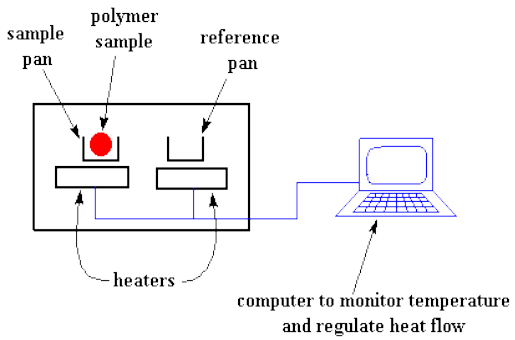

Fig. 3.16 *Schematic of a typical DSC unit.*

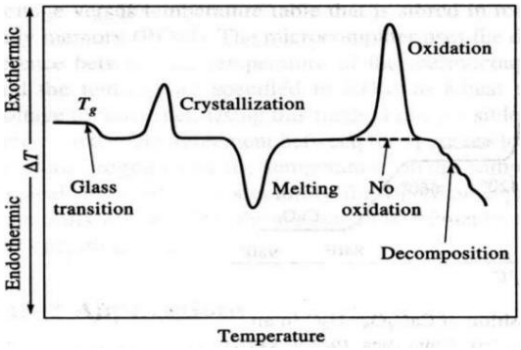

Fig. 3.17 *Schematic DSC curve.*

The heat capacity of a material is defined as the amount of heat required to raise the temperature to a certain value. Heat capacity is derived as,

$$\frac{q/t}{\Delta T/t} = \frac{q}{\Delta T} = C_p = heat\ capacity \qquad \textbf{(3.8)}$$

Heating a material leads to increase in its kinetic energy. In case of heating a polymer material, the molecular mobility is still restricted even though short range vibrations and rotations are present. On further heating the polymer converts in soft rubbery state. And this transition manifests in the form of an exothermic peak as shown in the figure. The corresponding temperature is termed as glass transition temperature (T_g). Further increasing the temperature leads to transition from rubbery state and an endothermic dip is observed as a consequence of it. The temperature at this conjecture is defined as melting temperature (T_m). DSC thus probes important phase transition phenomenon which can be interpreted to understand the thermodynamic nature of the material.

(SII EXSTAR-6000 DSC differential scanning calorimeter, SII SEIKO)

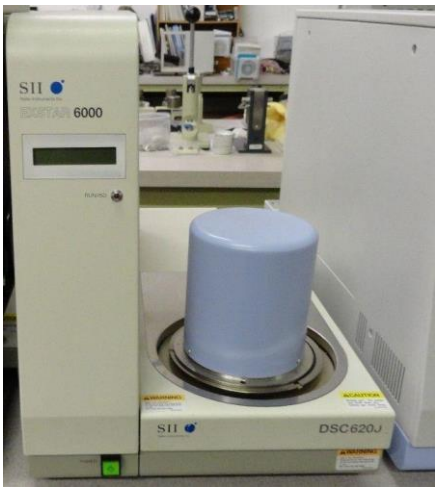

Fig. 3.18 *Image of DSC instrument.*

3.5 Transference Number Measurements

Ionic transport number is an important quantity to be measured to elucidate ion conduction mechanism occurring in the electrolyte materials. Various methods which are employed to measure the transport number in polymer electrolytes are Wagner's polarization technique, PEFG-NMR measurements, EMF measurements, potentiostatic polarization, Tubandt method and DC polarization technique ***(Wagner and Wagner, 1957; Saito et al., 1999; Evans et al., 1987; Robinson and Strokes, 2003; Kennedy, 1977; Tubandt and Anorg., 1920)***. Contribution of ionic conductivity in the total conductivity is measured by the transference number. Tubandt's method ***(Tubandt and Anorg., 1920)***, Hebb-Wagner's polarization method ***(Wagner and Wagner, 1957)*** and electrochemical (EMF) method ***(Evans et al., 1987)*** are commonly used methods for measuring the transference number. Some of these methods are briefly discussed below.

3.5.1 DC polarization technique

Evans et al (1987), suggested this method in which sodium amalgam was used. A typical cell in technique would be of the form ***Na- Hg | polymer electrolyte film | Na-Hg***. AC impedance measurements of the prepared cells, polarization of the cells and the measurement of ac impedance after polarization fall in order for measuring the transference number by this technique. The cells are polarized by applying a voltage $\Delta V = 20\text{mV}$ for 2h and the initial and final currents are recorded. Complex impedance

plots thus obtained are used to obtain the value of electrode-electrolyte contact resistances. The ionic transference number values are then calculated as

$$t_{Na} = \frac{I_S(\Delta V - R_0 I_0)}{I_0(\Delta V - R_S I_S)} \qquad (3.9)$$

where, I_0 and I_s are the initial and final currents andR_0, R_s are the cell resistances before and after polarization.

3.5.2 Wagner's polarization method

Fig. 3.18 shows schematic representation of the method. This method is commonly adopted to determine ionic and electronic transference numbers in a system. The sample is sandwiched between one blocking and one non-blocking electrode and polarized using a DC bias with constant voltage. Current is measured with respect to time at given dc potential.

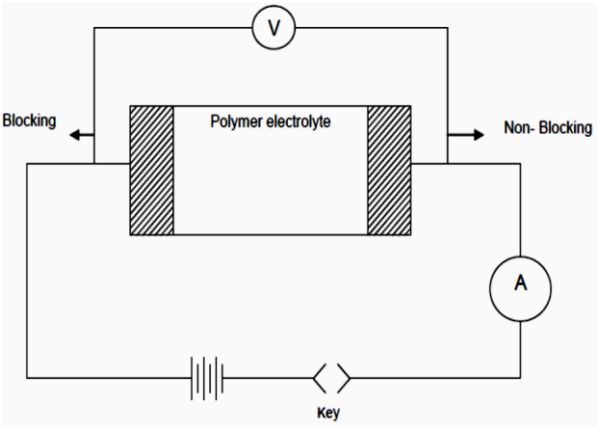

Fig. 3.19 *Wagner's Polarization method for transference number measurement Experimental setup.*

Following equations are employed to calculate electronic and ionic transference numbers respectively.

$$t_e = \frac{\sigma_e}{\sigma_T} = \frac{i_e}{i_T} \qquad (3.10)$$

$$t_i = i - t_e \qquad (3.11)$$

Initial current is the total current (i_T), due to the combination of ions (i_i) and electrons (i_e). With polarization built-up, i_i is blocked and finally only i_e survives. The initial total current decreases with time due to the reduction in ionic species of the electrolyte and exhausts completely where the residual current is only electronic in nature.

3.5.3 EMF method

In EMF method for transference number measurement, sample is placed between pair of electrodes having different chemical potentials μ_1 and μ_2. The potential difference (emf) developed across the electrodes is measured as,

$$E_{obs} = \frac{-1}{|Z|F}\int_{\mu_1}^{\mu_2} t_i d\mu = \frac{t_i(\mu_1 - \mu_2)}{|Z|F} = \frac{t_i \Delta G}{|Z|F} \qquad \textbf{(3.12)}$$

where t_i is the ionic transport number, μ_1 and μ_2 are chemical potential of the electrodes, ΔG is the change in free energy involved for a given pair of electrodes, $|Z|$ is the valency of mobile ion and F is Faraday's constant. An ideal electrolyte has $t_i = 1$ and the generated emf is given as,

$$E_{theo} = \Delta G/|Z|F \qquad \textbf{(3.13)}$$

From the above equations it is deduced that $E_{obs} = t_i \times E_{theo}$ and hence the ionic transference number is easily calculated as the ratio of observed emf E_{obs} to its theoretical value E_{theo}.

3.6 Complex Impedance Spectroscopy

Complex impedance analysis is exploited as one the most powerful techniques for investigating electrical properties of electrolytes. For the present studies, impedance measurements have been made on Agilent E4980A Precision LCR meter instrument, in the frequency range of 20 Hz-2 MHz from ambient temperature to 333 K. The sample is placed between two blocking silver electrodes (dia. = 1.2 cm) under spring pressure for impedance measurements. Conductivity and other related parameters such as the modulus and dielectric permittivity are studied using the complex impedance data. The real (Z') and imaginary (Z'') parts of the complex impedance, Z^*can be directly measured from the instrument. The complex impedance plot, also termed as Nyquist plot is obtained by plotting Z'' versus Z' graph. Bulk electrolyte resistance R_b and low frequency linear response are obtained from Nyquist plots by fitting to appropriate equivalent circuit using "*Zview2*" programme. Values of $R_b$are the used to calculate the ionic conductivity using the equation,

$$\sigma = \frac{1}{R_b} \times \frac{t}{A} \qquad \textbf{(3.14)}$$

where, t is the thickness of the sample and A is the area of the electrodes used. From the complex impedance Z^*, the dielectric permittivity and the complex modulus function are derived as,

$$\varepsilon^*(\omega) = \varepsilon'(\omega) - i\varepsilon'(\omega) = \frac{1}{i\omega C_0 Z^*} \quad \textbf{(3.15)}$$

$$M^*(\omega) = \frac{1}{\varepsilon^*(\omega)} = j\omega C_0 Z^* = M'(\omega) + jM''(\omega) \quad \textbf{(3.16)}$$

Electrode polarization is studied using the dielectric permittivity and the modulus function studies the conductivity relaxation process.

REFERENCES

1. L.A. Belfiore, *Physical Properties of macromolecules*, John Wiley & Sons, 2010.

2. R.A.V. Raff, A.S. Ahmad, *Northwest Sci.* 44 (1970) 184-205.

3. D.L. Dorest, *Characterization of solid Polymers*, S.J. Spells (ed.), Chapman & Hall, UK, 1994

4. P. Sharma, *Study of Conduction Mechanism in PEO-PMMA Polymer Blend Nano-composite Electrolytes*, Gujarat, India (2013).

5. J.Y. Kim, S.H. Kim, *Solid State Ionics*, 24 (1999) 91-99.

6. A. Virya, K. Lian, *Electrochemistry Communications*, 74 (2017) 33–37

7. Q. Tang, J. Wu, H. Sun, J. Lin, S. Fan, De Hu, *Carbohydrate Polymers*, 74 (2008) 215–219

8. R. Arunkumar, Ravi Shanker, M. Usha Rani, S. Rajendran, *Ionics* 23 (2017) 3097–3109.

9. S. Ramesh, K. H. Leen, K. Kumantha, A. K. Arof, *Spectrochimica Acta Part A: Mol. Biomol. Spectrosc.* 66 (2007) 1237–1242.

10. L. E. Amand, C.J. Tullin, *The Theory Behind FTIR analysis*, Department of Energy Conversion Chalmers University of Technology Goteborg, Sweden,1996.

11. J. B. Wagner and C. Wagner, *The Journal of Chemical Physics*, 26 (1957) 1957.

12. Y. Saito, H. Yamamoto, O. Nakamura, H. Kageyama, H. Ishikawa, T. Miyoshi, M. Matsuoka, *Journal of Power Sources*, 81-82(1999)772-776.

13. J.W. Evans, C.A. Vincent, P.G. Bruce, *Polymer*, 28 (1987) 2324-2328.

14. R. A. Robinson, R.H. Stokes, *Electrolyte Solutions*, Dover Publications, New York, 2003.

15. J. H. Kennedy, *Journal of Electrochemical Society* 124 (1977) 865.

16. C. Tubandt, Z. Anorg. *Allg. Chem.* 110 (1920) 234.